



OPEN ACCESS



Check for updates

Spiral wind-up of vortex sheets

H. Keith Moffatt^a and Yoshifumi Kimura^b^aDepartment of Applied Mathematics and Theoretical Physics, University of Cambridge, Cambridge, UK;^bGraduate School of Mathematics, Nagoya University, Nagoya, Japan

ABSTRACT

A model of the spiral wind-up of a vortex sheet by the flow induced by a perpendicular vortex is developed, first in the Euler limit of zero viscosity, then taking account of viscous diffusion. The wind-up of a vortex sheet by a propagating vortex pair is also considered; in this case, the vorticity grows exponentially near the two saddle points of the flow in the moving frame of the vortex pair. Estimates are obtained for the maximum vorticity ω_m and maximum enstrophy Ω_m attained through this process in terms of the wind-up Reynolds number Re and the initial dimensionless sheet thickness δ_0 . This paper is dedicated to Andrew Soward, whose sustained research in Dynamo Theory and Fluid Mechanics has been brilliantly inspiring for more than 50 years. Happy 80th, Andrew!

ARTICLE HISTORY

Received 23 July 2024

Accepted 7 September 2024

KEYWORDS

Navier–Stokes equations; exact solutions; vorticity amplification; Reynolds number saturation

1. Introduction

This paper is motivated by the fact that the mean rate of dissipation of energy $\Phi = \nu \langle \omega^2 \rangle$ in homogeneous turbulence appears to be independent of kinematic viscosity ν in the limit $\nu \rightarrow 0$ (the “dissipation anomaly”). If this is true, then the vorticity must exhibit singularities in the limit in order to provide infinite enstrophy $\Omega = \langle \omega^2 \rangle$. It has for long been believed that such singularities are associated with the intermittent concentrated vortices detected in direct numerical simulations (DNS) of turbulence (see for example Ishihara *et al.* 2009) and with the complex reconnection processes that such vortices may undergo (Melander and Hussain 1989). However, DNS of the reconnection of inclined vortex rings that approach each other under their mutual influence show very modest amplification of local vorticity at vortex Reynolds numbers up to about 4000 (Yao and Hussain 2020b). The analysis of (Moffatt and Kimura 2023) shows that during “Phase 1”, i.e. before the vortex cores begin to overlap and reconnect, the vorticity amplification is indeed modest at such Reynolds numbers, not greater than 2 (and only logarithmically dependent on the initial vortex core scale δ_0), so more complex mechanisms must be responsible for the much more intense vorticity amplification that is required.

Some of these more complex mechanisms are discussed in the extensive review by Yao and Hussain (2022) of vortex reconnection and its relevance for turbulence, which includes well over 100 references testifying to the historic and widespread interest in this problem.

CONTACT H. Keith Moffatt  hkm2@cam.ac.uk

© 2024 The Author(s). Published by Informa UK Limited, trading as Taylor & Francis Group. This is an Open Access article distributed under the terms of the Creative Commons Attribution-NonCommercial-NoDerivatives License (<http://creativecommons.org/licenses/by-nc-nd/4.0/>), which permits non-commercial re-use, distribution, and reproduction in any medium, provided the original work is properly cited, and is not altered, transformed, or built upon in any way. The terms on which this article has been published allow the posting of the Accepted Manuscript in a repository by the author(s) or with their consent.

In this review, the authors summarise their recent work (Yao and Hussain 2020a) on reconnection of perturbed anti-parallel vortices at Reynolds numbers up to 40,000. This shows much more dramatic increase of vorticity by a factor up to 500 or more during the reconnection process, when “bridges” of vorticity wind up rapidly around the perpendicular parent vortices. Similar intense amplification has been found by Kerr (2023) in DNS of the reconnection process for a single vortex initially in the form of a trefoil knot, when the intrinsic helicity of the knot can influence the details of the reconnection process. Exactly where and how this large intensification occurs remains quite obscure.

The spiral wind-up of bridge vortices by the parent vortices has led us to consider the model problem that is developed in §§ 3–7 below. Similar spiral wind-up has been considered previously by Gilbert (1988) who analysed the effect of a point vortex on a weak vortex patch by a two-dimensional treatment, linearised to the extent that the self-interaction of the distorted vortex patch was ignored; in this work, the vorticity was everywhere in the z -direction. [A model for the fine structure of turbulence involving strained spiral vortices had been developed earlier in the pioneering investigation of Lundgren 1982.] The key difference in the situation that we now consider is that the distorted vorticity is everywhere *perpendicular* to the vortex responsible for the distortion, and, as will be shown in § 2 below, no linearisation is required.

In §§ 3 and 4 viscosity is neglected, and pure Euler flow, for which vortex lines are frozen in the fluid, is considered. The effect of a propagating vortex pair on a vortex sheet is similarly analysed in § 5. Effects of viscosity (i.e. finite Reynolds number) are considered in §§ 6 and 7. Concluding comments are provided in § 8.

2. An elementary dual property of two-dimensional three-component flow

Consider first an incompressible velocity field of the form

$$\mathbf{u} = \mathbf{u}_1 + \mathbf{u}_2, \quad (1)$$

where

$$\mathbf{u}_1 = \{u_x(x, y, t), u_y(x, y, t), 0\} = \{\partial\psi/\partial y, -\partial\psi/\partial x, 0\}, \quad (2)$$

and

$$\mathbf{u}_2 = \{0, 0, u_z(x, y, t)\}. \quad (3)$$

The corresponding vorticity for such a “two-dimensional three-component” flow is

$$\boldsymbol{\omega} = \nabla \wedge (\mathbf{u}_1 + \mathbf{u}_2) = \boldsymbol{\omega}_1 + \boldsymbol{\omega}_2, \quad (4)$$

where

$$\boldsymbol{\omega}_1 = \{0, 0, \omega_z\} = \{0, 0, -\nabla^2\psi\}, \quad \boldsymbol{\omega}_2 = \{\partial u_z/\partial y, -\partial u_z/\partial x, 0\}. \quad (5)$$

The flows to be considered in subsequent sections fall within this general category.

The vorticity equation is

$$\partial \boldsymbol{\omega} / \partial t = \nabla \wedge (\mathbf{u} \wedge \boldsymbol{\omega}) + \nu \nabla^2 \boldsymbol{\omega}, \quad (6)$$

and the term $\nabla \wedge (\mathbf{u} \wedge \boldsymbol{\omega})$ responsible for advection and distortion of vorticity can be expanded as

$$\nabla \wedge (\mathbf{u} \wedge \boldsymbol{\omega}) = \nabla \wedge (\mathbf{u}_1 \wedge \boldsymbol{\omega}_1) + \nabla \wedge (\mathbf{u}_1 \wedge \boldsymbol{\omega}_2) + \nabla \wedge (\mathbf{u}_2 \wedge \boldsymbol{\omega}_1) + \nabla \wedge (\mathbf{u}_2 \wedge \boldsymbol{\omega}_2). \quad (7)$$

For such two-dimensional flows, invariant in the z -direction,

$$\nabla \wedge (\mathbf{u}_2 \wedge \boldsymbol{\omega}_1) = (\boldsymbol{\omega}_1 \cdot \nabla) \mathbf{u}_2 - (\mathbf{u}_2 \cdot \nabla) \boldsymbol{\omega}_1 = 0, \quad (8)$$

and

$$\nabla \wedge (\mathbf{u}_2 \wedge \boldsymbol{\omega}_2) = (\boldsymbol{\omega}_2 \cdot \nabla) \mathbf{u}_2 = \left\{ 0, 0, \frac{\partial u_z}{\partial y} \frac{\partial u_z}{\partial x} - \frac{\partial u_z}{\partial x} \frac{\partial u_z}{\partial y} \right\} = 0. \quad (9)$$

Hence

$$\nabla \wedge (\mathbf{u} \wedge \boldsymbol{\omega}) = \nabla \wedge (\mathbf{u}_1 \wedge \boldsymbol{\omega}_1) + \nabla \wedge (\mathbf{u}_1 \wedge \boldsymbol{\omega}_2). \quad (10)$$

The first term represents two-dimensional advection of the vorticity field $\boldsymbol{\omega}_1$ by its own self-induced velocity field \mathbf{u}_1 ; while the second term represents advection and distortion of the vorticity field $\boldsymbol{\omega}_2$ by the same \mathbf{u}_1 . Thus, \mathbf{u}_2 does not affect the 2D evolution of $\boldsymbol{\omega}_1$, and the vorticity $\boldsymbol{\omega}_2$ evolves under distortion by \mathbf{u}_1 alone (in conjunction with viscous diffusion). It is this dual property that we exploit in the following wind-up models.

3. Spiral wind-up of an initially plane vortex sheet in the Euler limit $\nu = 0$

The first situation to be considered [figure 1(a)] is the distorting effect of a ‘‘point’’ vortex of circulation Γ at $x = y = 0$ aligned with the z -axis, on a vortex sheet $\boldsymbol{\omega}_0 = \{\omega_0(y), 0, 0\}$ where $\omega_0(y)$ is at time $t = 0$ localised in the immediate vicinity of the plane $y/b = 1$; for example, $\omega_0(y)$ could be

$$\omega_0(y) = (U/(\sqrt{\pi} \delta_0)) \exp[-(y-b)^2/\delta_0^2] \quad (11)$$

with $\delta_0 \ll b$, in which case the associated velocity \mathbf{u}_0 satisfying $\nabla \wedge \mathbf{u}_0 = \boldsymbol{\omega}_0$ is

$$\mathbf{u}_0 = (U/2)\{0, 0, \operatorname{erf}[(y-b)/\delta_0] - c\}, \quad (12)$$

where U is the circulation per unit length of sheet in the x -direction, and c is a constant.¹ Choosing $c = 1$, the velocity rises from $-U$ below the sheet to zero above. This velocity, being uni-directional in the z -direction, has no effect on the point vortex, which remains steady at the origin, with associated velocity field

$$\mathbf{u}_1 = (\Gamma/2\pi r^2) \{-y, x, 0\}. \quad (13)$$

This circulating flow obviously distorts the vortex sheet, winding it up into a double spiral, as shown in figure 1(b).

¹ We ignore Kelvin–Helmholtz instability which would introduce variation in the z -direction, invalidating the simplicity of the present treatment.

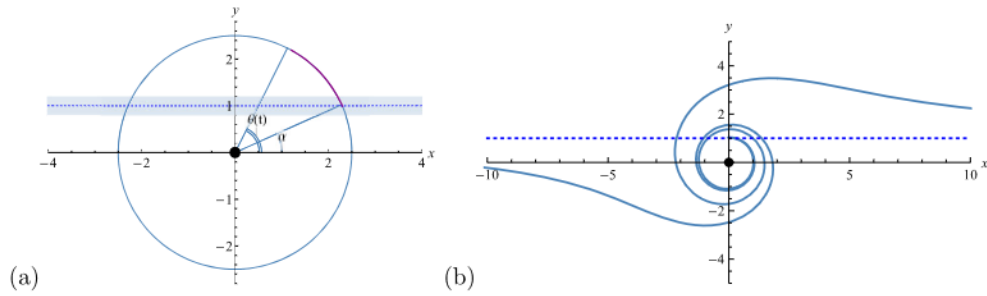


Figure 1. (a) Configuration sketch: the shaded strip around the dotted line $y = 1$ represents the vortex sheet at time $t = 0$, with vorticity in the x -direction, and the bullet point at the origin represents the point vortex; the material point initially at position $\{r, \alpha\}$ on the dotted line moves on the circle $r = \text{cst.}$ under the action of the point vortex to angle $\theta(t) = \alpha + t \sin^2 \alpha$; (b) the double-spiral form of the central vortex of the sheet at time $t = 4\pi$; at this stage, the leading point of the double spiral has made two complete revolutions round the point vortex (Colour online).

We adopt dimensionless variables, with b as the unit of length and $2\pi b^2 / \Gamma$ as the unit of time. Thus, we simply set $b = 1$ and $\Gamma/2\pi = 1$; with these choices, the Reynolds number, which we may describe as the “wind-up” Reynolds number, is simply $\text{Re} = \Gamma b^2 / 2\pi \nu = \nu^{-1}$.

Consider the material point that is at $\{X, y_0\}$ at time $t = 0$. In cylindrical polar coordinates, this point is $\{r, \alpha\}$, where

$$\alpha = \cot^{-1}(X/y_0) \quad \text{and} \quad r(\alpha, y_0) = \sqrt{y_0^2 + X^2} = y_0 \csc \alpha. \quad (14)$$

For $t > 0$, this material point moves on the circle $r = \text{cst.}$ to position $\{r, \theta\}$, where

$$\theta(\alpha, y_0, t) = \alpha + r^{-2}t = \alpha + t y_0^{-2} \sin^2 \alpha. \quad (15)$$

The cartesian coordinates of this particle at time t are therefore

$$x(\alpha, y_0, t) = y_0 \csc \alpha \cos [\alpha + t y_0^{-2} \sin^2 \alpha], \quad y(\alpha, y_0, t) = y_0 \csc \alpha \sin [\alpha + t y_0^{-2} \sin^2 \alpha]. \quad (16)$$

With parameter α , equation (16) define in parametric form the spiral shown in figure 1(b) for $y_0 = 1$, $t = 4\pi$.

Figures 2(a)–(d) shows, for $t = \pi/2, 2\pi, 8\pi$, and 16π , two adjacent vortex lines (blue and red) which start from the levels $y_0 = 1$ and $y_0 = 1.2$ respectively (these initial levels being marked by the dotted lines). The average length of these vortex lines over any interval of X ultimately increases linearly with time, the vorticity being correspondingly intensified. Note in figures 2(b),(c),(d) how the separation between the red and blue curves decreases as the central region is approached from either end; also, in figure 2(b), how the “leading point” of the blue vortex line rotates significantly faster [actually by a factor $(1.2)^2$] than that of the red one, because the former point starts nearer the origin.

These curves can equally be regarded as vortex lines on the isovorticity surfaces (all invariant in the z -direction). The flux of vorticity between these surfaces per unit length in the z -direction is constant, implying that the vorticity in the sheet also increases linearly

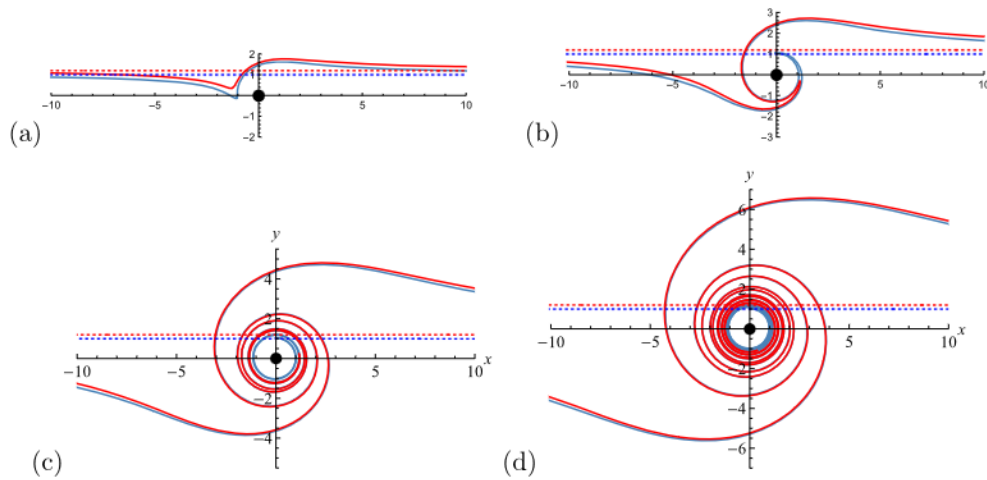


Figure 2. Frozen-field evolution of two vortex lines $\mathbf{x} = \mathbf{X}(\alpha, y_0, t)$ for $y_0 = 1$ (blue) and $y_0 = 1.2$ (red) under distortion by the point vortex (bullet point) at the origin; the initial positions are shown by the dotted lines; (a) $t = \pi/2$; (b) $t = 2\pi$; (c) $t = 8\pi$; (d) $t = 16\pi$; at this stage, the leading point of the blue spiral has made 8 complete turns round the origin, while that of the red spiral has made $8/(1.2)^2 \approx 5\frac{1}{2}$ turns (Colour online).

in the course of the wind-up. The velocity in the z -direction still jumps through the sheet from $-U$ on the “blue” side to zero on the “red” side, so that this velocity component becomes highly oscillatory as t increases; but this has no effect on the disturbing vortex which remains steady at the origin. Of course, in a real fluid, the increase of transverse velocity gradient is ultimately limited by viscous diffusion, which becomes stronger for so long as the average thickness of the vortex sheet decreases. This limiting effect of viscosity will be considered in § 6.

4. Spiral wind-up of an initially cylindrical vortex sheet in the Euler limit

$\nu = 0$

We may consider in a similar way the effect of a point vortex at the origin on an initial vortex sheet centred on a closed cylindrical surface. By way of example, consider the situation shown in figure 3(a), in which the vortex sheet at time $t = 0$ is located in a cylindrical annulus $x^2 + (y + b)^2 = a^2$ with $b = 1$ and $2.5 \lesssim a \lesssim 2.75$ (shaded grey in the figure), deliberately off-centred from the disturbing vortex (the extent b of this off-centering being here used as the unit of length). The vortex lines at $t = 0$ are concentric circles within this shaded annulus. Again, the blue and red curves [now closed, figures 3(b)–(d)] depict two initially adjacent vortex lines as t increases. In this case, a material point on the vortex sheet with parameter α ($0 \leq \alpha < 2\pi$) moves on the circle $r(\alpha, a) = \text{cst.}$, where now, from geometrical considerations,

$$r(\alpha, a) = -\sin \alpha + \sqrt{\sin^2 \alpha + a^2 - 1}, \quad (17)$$

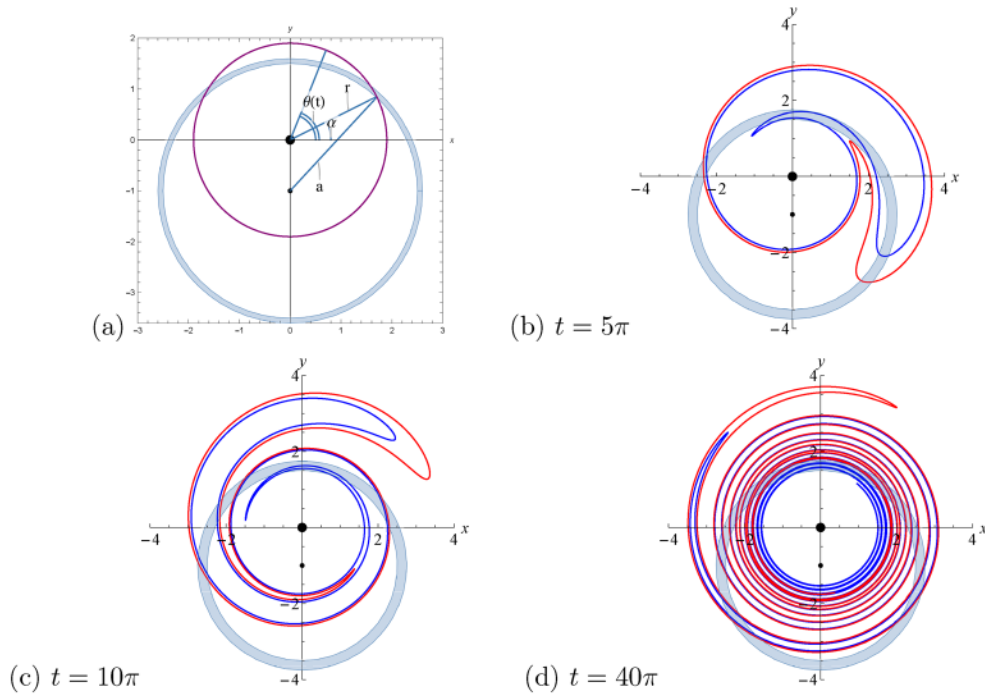


Figure 3. (a) Configuration sketch for initially circular vortex sheet, shown by the shaded circular annulus $x^2 + (y + 1)^2 = a^2$ with $2.5 < a < 2.75$; the small dot at $\{0, -1\}$ marks the centre of this circle. A material point with parameter α on the sheet moves on the upper circle [purple, radius $r(\alpha, a)$] with constant angular velocity $r(\alpha, a)^{-2}$. (b–d) Frozen-field evolution of two initially circular vortex lines in the vortex sheet [blue ($a = 2.5$) and red ($a = 2.75$)] under distortion by the point vortex (bullet) at the origin (Colour online).

and $\theta(\alpha, a, t) = \alpha + t/r(\alpha, a)^2$. The curves of figure 3(b)–(d) are now given in parametric form, for $a = 2.5$ (blue) and $a = 2.75$ (red), by

$$\mathbf{x} = \mathbf{X}(\alpha, a, t) = r(\alpha, a) \{ \cos [\theta(\alpha, a, t)], \sin [\theta(\alpha, a, t)] \}. \quad (18)$$

It is evident again that, under Euler evolution, the vortex sheet is distorted into a double spiral, which is ultimately confined between two circles of radii $\sim a_0 \pm 1$ (where a_0 is the initial mean radius of the sheet), a region of fixed area $A_0 \sim 4\pi a_0$.

The length $L(a, t)$ of these double spirals is given by

$$L(a, t) = \oint d|\mathbf{X}(\alpha, a, t)| = \int_0^{2\pi} \frac{d|\mathbf{X}(\alpha, a, t)|}{d\alpha} d\alpha. \quad (19)$$

This function is easily computed. Figure 4 shows that, as might be expected, $L(a, t)$ [computed here for $a = 2.5$ (blue) and 2.75 (red) to correspond with the curves of figure 3] grows linearly with time (after early transient behaviour), and under Euler evolution this stretching implies corresponding linear increase of mean vorticity; (the rate of growth for the red curve is less than that for the blue curve, reflecting the smaller average rate of strain that it experiences). Since the flux of vorticity between the red and blue curves of figure 3

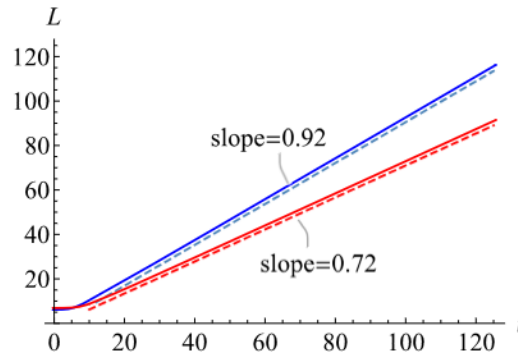


Figure 4. The length $L(a, t)$, given by equation (19) for $a = 2.5$ (blue) and $a = 2.75$ (red); in both cases, after a brief transient, the growth is linear, with asymptotic slopes indicated by the dashed lines (Colour online).

is constant, the mean separation between them decreases as t^{-1} after the initial transient phase, a behaviour ultimately limited by viscous diffusion (to be considered in § 6).

5. Sheet distortion by a vortex pair in the Euler limit $\nu = 0$

Consider now the evolution when two counter-rotating vortices of circulations $\pm\Gamma$ are placed at positions $\{\mp b, 0\}$ respectively (with $b = 1$), the initial vortex sheet being on a plane $y = y_0 > 0$, as in § 3. [This resembles a little more closely the spiral wind-up scenario encountered in vortex reconnection.] The vortex pair propagates with velocity $\frac{1}{2}$ in the y -direction, so that, in the frame of reference moving with this vortex pair, there is a uniform stream $\{0, -\frac{1}{2}\}$ at infinity. The stream-function for the steady flow in the $\{x, y\}$ plane in this moving frame is then

$$\psi(x, y) = \frac{1}{2}x - \log[r_1/r_2], \quad \text{where } r_{1,2} = (x \pm 1)^2 + y^2, \quad (20)$$

and the distorting velocity field $\mathbf{u}_1(x, y)$ is given by

$$\mathbf{u}_1(x, y) = \{\partial\psi/\partial y, -\partial\psi/\partial x, 0\}. \quad (21)$$

The streamlines of this flow in the $\{x, y\}$ plane are shown in blue in figure 5; note particularly the two saddle points S_1 and S_2 at positions $\{0, \pm\sqrt{3}\}$, and the boundary C (which contains S_1 and S_2) of the region of closed streamlines. Near each saddle point, the flow is one of uniform irrotational strain

$$\mathbf{u}_1(x, y) \sim (\sqrt{3}/4)\{x, -(y - \sqrt{3})\} \quad \text{near } S_1, \quad (22)$$

and

$$\mathbf{u}_1(x, y) \sim (\sqrt{3}/4)\{-x, (y + \sqrt{3})\} \quad \text{near } S_2. \quad (23)$$

Thus, material lines are stretched exponentially in the x -direction near S_1 , and in the y -direction near S_2 .

The vortex sheet is carried by this flow, and the behaviour depends on whether the initial level $y = y_0$ is greater or less than $\sqrt{3} \approx 1.732$. For example, a material line initially at $y = 3$

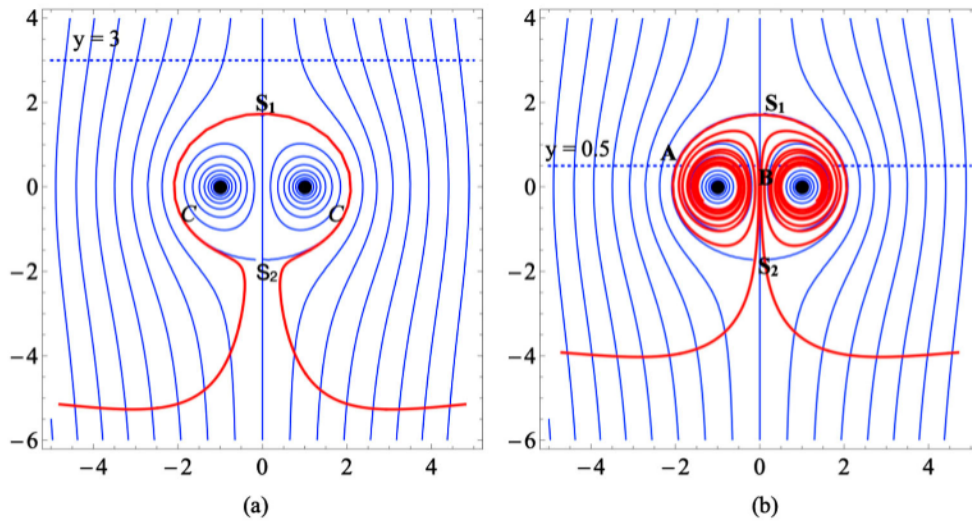


Figure 5. Streamlines (blue) of the flow due to point vortices $\pm\Gamma$ at $(\mp 1, 0)$ (marked by the bullets) in the frame moving with the vortices; there are saddle points at S_1 and S_2 , and the (double) streamline C through these points bounds two regions of closed streamlines. (a) The vortex sheet is initially at level $y = 3$ and moves downwards with the flow; it is shown in red at $t = 15$ by which time it embraces the curve C forming the shape of an Ω . (b) The vortex sheet is initially at level $y = 0.5$, intersecting C at A (which moves towards S_2) and the axis of symmetry at B (which moves towards S_1), with symmetric development on both sides; the vortex sheet is shown in red at time $t = 8$ by which time two double-spirals have been formed (Colour online).

[figure 5(a)] will be drawn down (uniformly for $|x| \gg 1$) but cannot cross C ; it must wrap around this curve, although taking a logarithmically infinite time to reach the saddle point S_1 , and so an infinite time to actually make contact with C . However it will achieve this more and more closely as time increases, the form of the sheet resembling an Ω with tails extending to $\pm\infty$ during the late stage of evolution; (the behaviour is quite similar to that first encountered by Maxwell (1870), in consideration of the transport of material points by potential flow past a circular cylinder). The vorticity in the vortex sheet of figure 5(a) must increase exponentially in the neighbourhood of S_1 , until limited by viscosity.

By contrast, a vortex sheet placed initially at level $y = 0.5$ [figure 5(b)] which intersects C at the point A and the x -axis at B behaves quite differently. The material particle at A moves down the streamline C towards the lower stagnation point S_2 while the material particle at B moves up the axis towards S_1 ; (the behaviour is of course symmetric about the plane $x = 0$). Between these moving points, the vortex sheet is deformed to two double-spirals because of the shear in the flow around the point vortices, just as in § 3, the difference being that here, the material points A and B ultimately approach very near S_2 and S_1 respectively, and are then in effect “pinned” in these immediate neighbourhoods. Outside C , the two external branches of the vortex sheet must ultimately approach each other closely near S_2 forming a spike at this point. In this neighbourhood the vorticity intensifies exponentially in the y -direction, until again limited by viscosity. Reconnection is then to be expected near S_2 , allowing the external portion of the sheet to detach and continue to move downwards (in the frame of the vortex pair); the internal double-spirals must then continue to evolve in Phase 2 and Phase 3, much as described in § 3 above.

6. Finite Reynolds number effect

Viscous diffusion must ultimately intervene as the length-scale transverse to the deforming vortex sheet decreases. If we limit attention to the simple case treated in § 4 above, this scale decreases like $[|\alpha(r)|t]^{-1}$, where $\alpha(r)$ is the local shear rate in the flow due to the point vortex,² while the length of any portion of the sheet increases linearly in t . At the same time, although the sheet is being stretched and therefore tending to decrease in thickness, this is counteracted (and ultimately dominated, as shown below) by viscous diffusion which tends to increase the lateral spread of the sheet. These competing effects are well illustrated by the following simple model (an exact solution of the Navier–Stokes equation).

Consider a vortex sheet given by $\omega = \{0, \omega(x, t), 0\}$, under the condition that at time $t = 1$,

$$\omega(x, 1) = \omega_0 \exp[-x^2/\delta_0^2], \quad \text{where } \omega_0 = U/(\sqrt{\pi} \delta_0); \quad (24)$$

thus U is the jump in the (z -component of) velocity across the sheet (figure 6). Suppose that this sheet is subjected for $t > 1$ to the unsteady irrotational strain field³

$$\mathbf{U}_s(t) = \{-\alpha(t)x, \alpha(t)y, 0\} \quad \text{where } \alpha(t) = t^{-1}. \quad (25)$$

For this model problem, $\omega(x, t)$ satisfies the equation

$$\frac{\partial \omega}{\partial t} - \alpha(t)x \frac{\partial \omega}{\partial x} = \alpha(t)\omega + \nu \frac{\partial^2 \omega}{\partial x^2}, \quad (26)$$

where ν is the kinematic viscosity of the fluid. Since the flux of vorticity per unit length of sheet in the z -direction, U , must remain constant, we may seek a solution of (26) of the form

$$\omega(x, t) = \omega(t) \exp[-x^2/\delta(t)^2], \quad \text{with } \omega(t) = U/[\sqrt{\pi} \delta(t)]. \quad (27)$$

Substituting in (26) and rearranging leads to the equation

$$\frac{U}{\sqrt{\pi} \delta^3} \left[\delta \frac{d\delta}{dt} + \alpha(t)\delta^2 - 2\nu \right] \left(1 - \frac{2x^2}{\delta^2} \right) \exp \left[-\frac{x^2}{\delta(t)^2} \right] = 0. \quad (28)$$

Since this must be satisfied for all x , it follows that, with $\alpha(t) = 1/t$,

$$\frac{d}{dt} \delta^2 + \frac{2\delta^2}{t} = 4\nu. \quad (29)$$

The solution of this equation satisfying the condition $\delta(1) = \delta_0$ is

$$\delta^2/\delta_0^2 = t^{-2} + \epsilon(t-1) \quad \text{with } \epsilon = 4\nu/3\delta_0^2, \quad (30)$$

² With $v(r) = r^{-1}$, the local shear rate is $\alpha(r) = rd(v/r)/dr = -2/r^2$. For the relevant range $1.5 \lesssim r \lesssim 2.5$ in figure 3, $|\alpha(r)|$ varies between 0.89 and 0.32; for order of magnitude purposes, we simply adopt the value $|\alpha| = 1$ in the estimates that follow.

³ This choice mimics the strain that the same vortex sheet would experience under a constant shear flow $\{a y, 0, 0\}$, which would rotate the sheet for large t to a decreasing angle $\theta(t) = \tan^{-1}(\alpha t)^{-1} \sim (\alpha t)^{-1}$ that the sheet would make with the plane $y = 0$ (see figure 6). Under the strain (25) with $\alpha = t^{-1}$ (for $t > 1$), the stretching of material line elements is linear in time, in contrast to the exponential stretching that occurs under *constant* irrotational strain.

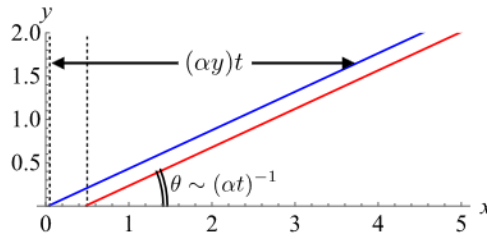


Figure 6. Sketch illustrating how, while two material lines are subjected to the shear $\{\alpha y, 0\}$, the separation between them decreases as $(\alpha t)^{-1}$ (Colour online).

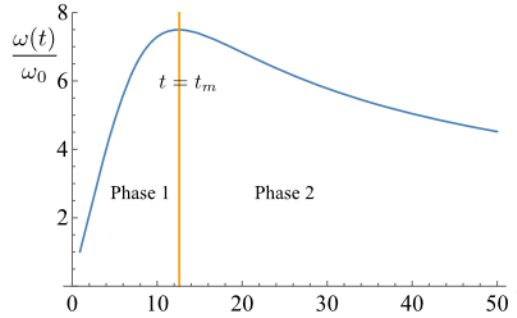


Figure 7. The function $\omega(t)/\omega_0$ for $t > 1$ and $\epsilon = 10^{-3}$ as given by equation (31). The curve is maximal at $t = t_m \approx 12.6$, separating two stages of evolution: Phase 1 (essentially inviscid vortex stretching), and Phase 2 (when viscous decay dominates) (Colour online).

and the corresponding vorticity distribution is then given by (27). The amplification of vorticity is given by

$$\frac{\omega(t)}{\omega_0} = \frac{\delta_0}{\delta(t)} = [t^{-2} + \epsilon(t-1)]^{-1/2}. \tag{31}$$

This is maximal when $t = t_m = (2/\epsilon)^{1/3}$, at which time $\omega(t_m) = \omega_m$ and

$$\frac{\omega_m}{\omega_0} = [2^{1/3} + 2^{-2/3}]^{-1/2} \epsilon^{-1/3} \approx 0.727 \epsilon^{-1/3} \approx 0.661 \delta_0^{2/3} \text{Re}^{1/3}. \tag{32}$$

The situation is illustrated in figure 7, which shows $\omega(t)/\omega_0$ as a function of t , for the choice $\epsilon = 10^{-3}$. There are here essentially two phases: Phase 1, during which viscosity is negligible and the vorticity in the sheet (at the central plane $x = 0$) grows linearly, as expected in Euler evolution; and Phase 2, during which viscous diffusion more than compensates the stretching effect, and the central vorticity decays slowly as $t^{-1/2}$. Note that during Phase 2 (when $t \gg 1$), $\delta^2 \sim 4\nu t/3$, a factor 1/3 less than the growth rate $4\nu t$ that would hold if the straining $\alpha(t) = t^{-1}$ were absent: the strain retards the increase of sheet thickness (and the corresponding decay of vorticity), but viscosity still dominates.

Approach of two sheared vortex sheets

The above discussion relates to a single vortex sheet in isolation, but in the spiral wind-up situation, oppositely directed portions of the spiral vortex sheet approach each other

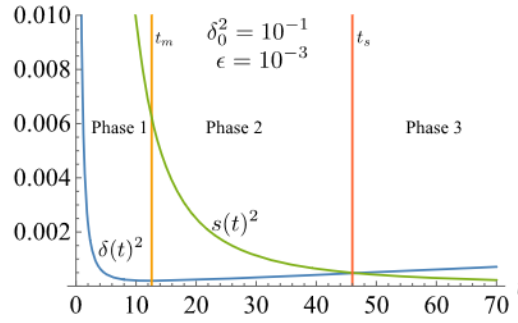


Figure 8. The functions $\delta(t)^2$ (minimal at $t = t_m$) and $s(t)^2 = t^{-2}$, which cross at $t = t_s \approx 46$; at this stage, oppositely directed portions of the folded spiral sheets begin to overlap, and rapid decay ensues; this defines the onset of Phase 3 (Colour online).

under the shearing that both portions experience.⁴ The separation of such portions, $s(t)$, decreases as $|\alpha(r)|t^{-1}$ and is ultimately of the same order as $\delta(t)$ (see figure 8). At this stage, taking $|\alpha(r)| \sim 1$, $\delta^2 \sim \delta_0^2(t^{-2} + \epsilon t)$, so that $s^2 \sim \delta^2$ when $\delta_0^2(t^{-2} + \epsilon t) \sim t^{-2}$, or, since $\delta_0 \ll 1$, when

$$t \sim t_s = (\delta_0^2 \epsilon)^{-1/3} \sim \nu^{-1/3}. \quad (33)$$

[With the choices $\delta_0 = 10^{-1}$, $\epsilon = 10^{-3}$, this gives $t_s = 10^{5/3} \approx 46$, as indicated quite accurately in figure 8.]

From this point on, the overlapping of adjacent folded sheet layers with their opposed directions of vorticity presumably leads to more rapid decay of vorticity, possibly involving complex reconnection processes and transition to turbulence, which we do not seek to analyse here. We denote this terminal phase as Phase 3.

7. Growth of enstrophy

We can now estimate the rate of growth of enstrophy, based on the above results. For this purpose, we again focus on the case of § 4, the spiral wind-up of a cylindrical vortex sheet, and we adopt the mean over the fixed area $A_0 \sim 4\pi a$, to which the vorticity is ultimately confined. During Phase 1, the length of the sheet and the vorticity within it increase linearly in time, but the thickness of the sheet decreases as t^{-1} , so that the sub-area A of the xy -plane over which the vorticity is significant remains constant. It follows that, during this phase, the enstrophy $\Omega(t)$ behaves like

$$\Omega(t) = A_0^{-1} \int_{A_0} \omega^2 dA = A_0^{-1} \int_A \omega^2 dA \sim (A/A_0) \omega_0^2 t^2. \quad (34)$$

During Phase 2, the length continues to increase linearly, but the thickness δ increases as $t^{1/2}$ so that $A \sim t^{3/2}$, and the vorticity ω in the sheet decreases as $t^{-1/2}$. Hence, during this

⁴ At the same time, the distorting vortex will diffuse as a Lamb vortex, and its distorting effect will diminish when $\nu t \gtrsim 1$.

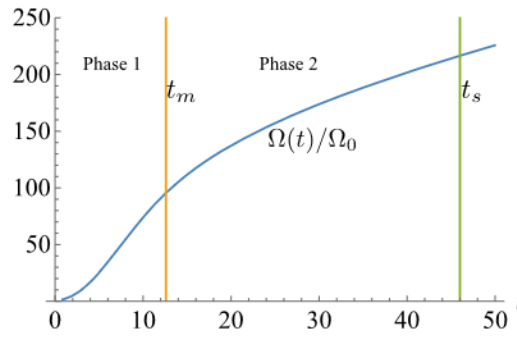


Figure 9. The function $\Omega(t)/\Omega_0$ (for $\delta_0 = 10^{-1}$, $\epsilon = 10^{-3}$) given by (36), which increases as t^2 during Phase 1, then as $(t/\epsilon)^{1/2}$ during Phase 2 (Colour online).

phase,

$$\Omega(t) \sim (A(t)/A_0)\omega_0^2 t^{-1} \sim A_0^{-1}\omega_0^2 t^{-1}t^{3/2} = A_0^{-1}\omega_0^2 t^{1/2}. \quad (35)$$

This increase continues only until the time $t \sim t_s$ when counter-directed portions of the sheet overlap and engage in mutual annihilation.

More accurately, using the results (30) and (31), we have

$$\Omega(t)/\Omega_0 = t[(t^{-2} + \epsilon(t-1))]^{-1/2}. \quad (36)$$

This function is shown in figure 9 in which the t^2 growth in Phase 1 giving way to the $t^{1/2}$ growth in Phase 2 is apparent. Note that Ω continues to grow as $t^{1/2}$ in Phase 2 although ω decreases as $t^{-1/2}$.

When $t \sim t_s = (\delta_0^2 \epsilon)^{-1/3}$, at which time $\Omega(t)$ reaches its maximum Ω_m , using (30) we find

$$\Omega_m/\Omega_0 \sim (\delta_0 \epsilon^2)^{-1/3} \sim \delta_0 \nu^{-2/3}, \quad \text{or equivalently } \Omega_m \sim U^2 \nu^{-2/3}. \quad (37)$$

For example, if $\delta_0 = 10^{-1}$ and $\epsilon = 10^{-3}$, this gives $\Omega_m/\Omega_0 \sim 10^{7/3} \approx 215$, a very significant level. Note that at this stage, ω^2 is spread over the whole area A_0 ; as $\nu \rightarrow 0$, the vorticity becomes singular over this whole area (like $\delta_0^{1/2} \nu^{-1/3}$). However, the maximum of the mean rate of dissipation of energy, $\Phi_m = \nu \Omega_m$, behaves as

$$\Phi_m \sim \Omega_0 \delta_0 \nu^{1/3}, \quad (38)$$

and this tends to zero as $\nu \rightarrow 0$; there is thus no dissipation anomaly in this situation.

Enstrophy growth for the vortex-pair problem of § 5

The vortex-pair problem of § 5 calls for special consideration, given the exponential behaviour near the saddle points. For this purpose, let Ω_0 now represent the initial enstrophy (per unit length in the z -direction) in the section of the initial vortex sheet that ultimately wraps itself round the closed curve C [figure 5]; the length of this section is of order unity. The vorticity in the sheet is $O(U\delta_0^{-1})$ and its thickness is $O(\delta_0)$; hence $\Omega_0 = O(U^2 \delta_0^{-2} \delta_0) = O(U^2 \delta_0^{-1})$. When $\nu > 0$, the vorticity in the neighbourhood of S_1 presumably asymptotes to a steady vortex sheet as given by equation (11) (here with

$b = \sqrt{3}$ and $\delta^2 = 8\nu/\sqrt{3}$ [as adopted by Townsend 1951 in his early model of the dissipative structures of turbulence]. The contribution to the asymptotic enstrophy from an $O(1)$ section of the closed curve C centred on S_1 is therefore $\Delta\Omega = O(U^2\delta^{-1}) = O(U^2\nu^{-1/2})$.

When $y_0 > \sqrt{3}$ [figure 5(a)] (and if $\delta \ll \delta_0$) this $\Delta\Omega \sim \delta_0/\delta$ is presumably in order of magnitude the dominant contribution to the maximum increase in enstrophy.

When $y_0 < \sqrt{3}$ [figure 5(b)], taking $\Omega_m \sim U^2\nu^{-2/3}$ [as in equation (37)] to be the contribution to enstrophy from the wind-up region interior to C , $\Delta\Omega/\Omega_m \sim \nu^{-1/2}\nu^{2/3} = \nu^{1/6}$, so that $\Delta\Omega \ll \Omega_m$ in the limit $\nu \rightarrow 0$. However, this “surface contribution” may survive for long after the time $t \approx t_s$ when the “internal contribution” to the enstrophy Ω is dissipated on this same time-scale $t_s \sim \nu^{-1/3}$ (cf Rhines and Young 1983).

These conclusions are tentative, and require verification by more extensive computations than we have undertaken here.

8. Discussion

We have developed a model of the spiral wind-up of a vortex sheet, either one of infinite extent (§ 3) or one that is initially cylindrical in form (§ 4). We have also considered the behaviour when a vortex sheet is deformed by the flow induced by a propagating vortex pair (§ 5). We have obtained estimates of the maximum vorticity ω_m (§ 6) and maximum enstrophy Ω_m (§ 7) that are attained before viscosity limits their growth. The results may have a bearing on the problem of vortex reconnection, which in some respects continues to defy analysis and physical understanding. Although the enstrophy $\Omega_m \sim \nu^{-2/3}$ becomes unbounded as $\nu \rightarrow 0$, the mean rate of dissipation of energy $\nu\Omega_m \sim \nu^{1/3}$, tends to zero in the limit, so there is no “dissipation anomaly” in the situations considered. Nevertheless, just as Gilbert’s (1988) two-dimensional spiral wind-up model had relevance for two-dimensional turbulence, so the present model may have relevance for three-dimensional turbulence in which randomly distributed concentrated vortex tubes will always tend to wind up any local vortex sheets in their vicinity.

Some generalisations of the problem considered here deserve investigation. First, it is clear that any distribution of point vortices could be considered to provide the “distorting velocity field” $\mathbf{u}_1(x, y, t)$. Two co-rotating vortices could be easily treated, much as in § 7. Three or more vortices can lead to chaotic particle paths (Aref 1983), and hence presumably to exponential growth of vorticity in regions of chaos until limited by viscosity, a possibility that deserves investigation.

Secondly, the axisymmetric counterpart of the present theory also invites attention. Thus for example, a circular concentrated vortex will, as it propagates, deform a vortex sheet on a surrounding torus having the same axis of symmetry, in a manner that should admit treatment similar to that presented in this paper. Here, we would be dealing with an axisymmetric flow with a swirl component. Vortex sheets confined to a torus have been previously envisaged (Moffatt 1984), but here we would have the additional ingredient of a poloidal flow deforming the poloidal vorticity.

Finally, we should note that, despite the familiar analogy between vorticity in Euler flows and magnetic field in ideal fluids, there is no simple magnetohydrodynamic counterpart of the situations considered in this paper. The reason is that a deformed magnetic sheet (analogous to the deformed vortex sheet of § 3) would be subject to a non-zero restoring

Lorentz force associated with the Maxwell tension in the magnetic field lines. There is no corresponding restoring force for the vorticity problem, as is evident from the preliminary discussion of § 2.

Disclosure statement

No potential conflict of interest was reported by the author(s).

Funding

We thank the Isaac Newton Institute for Mathematical Sciences, Cambridge, for support and hospitality during the programme *Anti-diffusive dynamics: from sub-cellular to astrophysical scales* (supported by EPSRC grant EP/R014604/1), when work on this paper was undertaken. We also acknowledge the valued use of *Mathematica* in the production of the graphics. Y.K. acknowledges support from JSPS KAKENHI, grant nos. 19H00641 and 22K18768. And finally, we thank two referees, whose suggestions have led to significant improvements in the paper.

References

- Aref, H., Integrable, chaotic, and turbulent vortex motion in two-dimensional flows. *Annu. Rev. Fluid Mech.* **1983**, **15**, 345–389.
- Gilbert, A.D., Spiral structures and spectra in two-dimensional turbulence. *J. Fluid Mech.* **1988**, **193**, 475–497.
- Ishihara, T., Gotoh, T. and Kaneda, Y., Study of high-Reynolds number isotropic turbulence by direct numerical simulation. *Annu. Rev. Fluid Mech.* **2009**, **41**, 165–180.
- Kerr, R.M., Sensitivity of trefoil vortex knot reconnection to the initial vorticity profile. *Phys. Rev. Fluids* **2023**, **8**, 074701.
- Lundgren, T.S., Strained spiral vortex model for turbulent fine structure. *Phys. Fluids* **1982**, **25**, 2193–2203.
- Maxwell, J.C., On the displacement in a case of fluid motion. In *Scientific Papers of James Clerk Maxwell*, **2**, pp. 208–214, 1870 (Cambridge University Press).
- Melander, M.V. and Hussain, F., Cross-linking of two antiparallel vortex tubes. *Phys. Fluids A: Fluid Dyn.* **1989**, **1**, 633–636.
- Moffatt, H.K., Simple topological aspects of turbulent vorticity dynamics. In *Turbulence and Chaotic Phenomena in Fluids*, Elsevier. *Proc. IUTAM Symposium, Kyoto, Sept. 1983*, edited by T. Tatsumi, pp. 223–230, 1984.
- Moffatt, H.K. and Kimura, Y., Towards a finite-time singularity of the Navier–Stokes equations. Part 3. Maximal vorticity amplification. *J. Fluid Mech.* **2023**, **967**, R1.
- Rhines, P.B. and Young, W.R., How rapidly is a passive scalar mixed within closed streamlines? *J. Fluid Mech.* **1983**, **133**, 133–145.
- Townsend, A.A., On the fine-scale structure of turbulence. *Proc. R. Soc. A* **1951**, **208**, 534–542.
- Yao, J. and Hussain, F., A physical model of turbulence cascade via vortex reconnection sequence and avalanche. *J. Fluid Mech.* **2020a**, **883**, A51.
- Yao, J. and Hussain, F., On singularity formation via viscous vortex reconnection. *J. Fluid Mech.* **2020b**, **888**, R2.
- Yao, J. and Hussain, F., Vortex reconnection and turbulence cascade. *Annu. Rev. Fluid Mech.* **2022**, **54**, 317–347.